Epitaxial Growth of Nanorod Meshes from Luminescent Organic Cocrystals via Crystal Transformation

Yanqiu Sun,[†] Yilong Lei,[*‡] Wenping Hu,[‡] and Wai-Yeung Wong[*†]

[†]Department of Applied Biology and Chemical Technology, The Hong Kong Polytechnic University (PolyU), Hung Hom, Hong Kong, P. R. China and PolyU Shenzhen Research Institute, Shenzhen, 518057, P. R. China

[‡]Department of Chemistry, School of Science, Tianjin University, Tianjin, 300072, P. R. China

Supporting Information Placeholder

ABSTRACT: Two-dimensional (2D) nanorod meshes made of benzoperylene-1,3-dicyanotetrafluorobenzene (BP-1,3-DTFB) were formed via crystal transformation of the pre-existing BP microsheets. The transformation was driven by cooperative effect of intermolecular charge-transfer (CT) and arene-fluoroarene (AF) interactions. Epitaxial growth of cyan-emitting BP-1,3-DTFB nanorod meshes is directed by small lattice mismatch between BP and BP-1,3-DTFB, followed by the consumption of BP and the formation of BP-1,3-DTFB. Such a crystal transformation strategy can also be used to guide the formation of BP-1,4-dicyanotetrafluorobenzene (BP-1,4-DTFB) nano-meshes. The present work reports a simple yet effective approach for the realization of aligned organic nanorod superstructures.

Ordered nanorod/nanowire arrays made of π-conjugated molecules have received considerable attentions because of their superior performance applications in photonics and electronics, such as high-efficiency light-emitting transistors.[1] In contrast to individual nanorods with random orientations, nanorod arrays possess large surface area, tailorable densities, and specific orientations, thus giving enhanced optoelectronic performances. Notably, aligned nanostructures commonly exhibit a vertical or horizontal orientation, which are formed by different synthetic methodologies. For instance, a prototype organic semiconductor, 9,10-bis(phenylethynyl)anthracene (BPEA), was arranged into vertically nanowire arrays on a graphene substrate via van der Waals (vdWs) epitaxial strategy, which serve as optical waveguiding media or microcavity.[1b] Beyond that, BPEA also assembled into horizontal nanowire arrays via physical vapor transport (PVT) or a drop-casting method,[3] which either present strong waveguiding ability with photon propagation distance up to 180 μm[3a] or act as high efficiency field-effect transistor devices.[3b] However, these successful demonstrations mainly focus on one-dimensional (1D) aligned rods/wires. To date, rational synthesis of two-dimensional (2D) organic nanorod superstructures still remains an unsolved problem due to the greater structural complexity.

Fortunately, a few relevant works on 2D inorganic nanorod meshes have been realized in Bi-containing or fullerene (C_{60})-based systems.[4] For example, crystalline β-Bi_2O_3 thin films undergo sequential crystal transformation to form 2D nested Bi_2S_3 network superstructures.[4a,b] The network alignment is determined depending on epitaxial relationships among diverse Bi compounds. The key to achieve this involves the formation of 2D sacrificial template and subsequent epitaxial growth of aligned nanorods.[4] Inspired by these successes, we aim to access similar 2D network superstructures from π-conjugated molecules, where preformed organic microsheets evolve into ordered nanorod arrays.

Herein, we report a simple crystal transformation strategy for epitaxial growth of nanorod meshes comprising benzoperylene-1,3-dicyanotetrafluorobenzene (BP-1,3-DTFB) (Figure 1). Specifically, single-crystall`ine BP microsheet template was first achieved, followed by the spontaneous dissolution and the formation of oriented BP-1,3-DTFB nanorods. Such a

transformation process is triggered by cooperative intermolecular interactions between BP and 1,3-DTFB. Desired epitaxial relationship between them directs oriented growth of BP-1,3-DTFB. The present crystal transformation strategy can also be used to achieve BP-1,4-DTFB nano-meshes, indicating its effectiveness. This work provides an ideal platform for in-depth understanding of the construction of ordered nanorod superstructures.
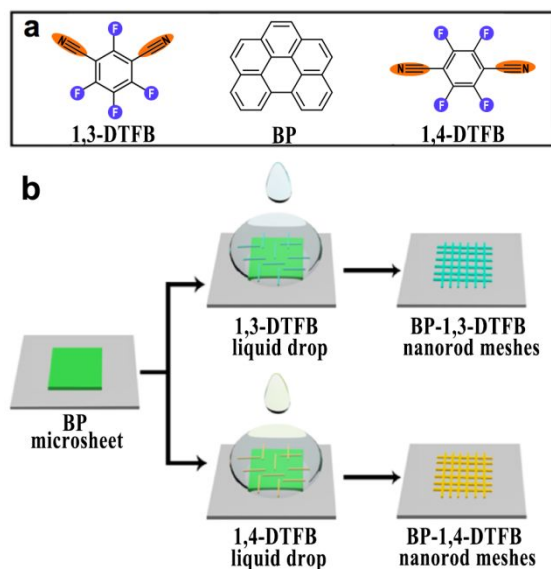

Figure 1. (a) Molecular structures of electron D/A pairs. (b) Schematic representation of BP-based nanorod meshes formed via crystal transformation of BP microsheets.

We selected BP and fluorinated 1,3-DTFB as an electron donor/acceptor (D/A) pair based on the following considerations: (1) Similar to the case of perylene (Pe),[5] BP has also a tendency to form sheet-like appearance, as verified by the morphology simulation result (Figure S1). (2) Cooperative intermolecular interactions, i.e. charge-transfer (CT)[6] and arene-fluoroarene (AF) interactions[7], may co-exist in BP-1,3-DTFB cocrystal considering that 1,3-DTFB contains multiple electron withdrawing groups (fluorine atoms and cyano groups). To achieve nanorod meshes, 2D microsheets need to be first prepared and serve as a template. Specifically, BP microsheets were formed by slow evaporation of BP solution in toluene ($C_{BP} = 30$ mM). As confirmed by the scanning/transmission electron microscopy (SEM/TEM, Figure 2a, b) results, BP assembles into smooth microsheets with an average width of around 150 μm, suggesting its high crystallinity. The selected-area electron diffraction (SAED) pattern of a typical square microsheet (inset in Figure 2b) clearly confirms its single-crystalline nature. Combined with the crystallographic data (Table S1), we infer that BP sheets grow along [110] and [1-10]

directions. Under UV excitation, BP microsheets present strong green light at the edges (Figure 2c).

Moreover, BP-1,3-DTFB wires were also synthesized by a drop-casting method. Typically, a drop of BP/1,3-DTFB solution with equimolar ratio ($C_{BP} = C_{DTFB} = 50$ mM) was rapidly dried on a substrate. Instead of 2D microsheets, 1D microwires were obtained (Figure 2d, e), indicating the formation of BP-1,3-DTFB cocrystal. For comparison, rod-like BP-1,3-DTFB crystal suitable for single-crystal X-ray diffraction (SCXRD) was also achieved by slow evaporation of BP/1,3-DTFB solution in THF. Notably, X-ray crystallographic analysis reveals that the monoclinic binary cocrystal is composed of BP and 1,3-DTFB with 1:1 stoichiometry. In such a cocrystal, BP and 1,3-DTFB molecules are stacked alternately in a parallel manner (Figures S2, S3). As simulated by Material Studio software (Figure S5), 1D morphology of BP-1,3-DTFB is achieved as a result of intermolecular CT and AF interactions, which matches well with the above wire-like appearance. The SAED pattern of single BP-1,3-DTFB microwire reveals that they were grown along [100] direction (inset in Figure 2f). Under UV excitation, BP-1,3-DTFB microwires emit stronger cyan light with a photoluminescence quantum yield (PLQY) of 18.9% (Figure 2d), when compared to the green-emitting BP microsheets with a PLQY of 10.0%.
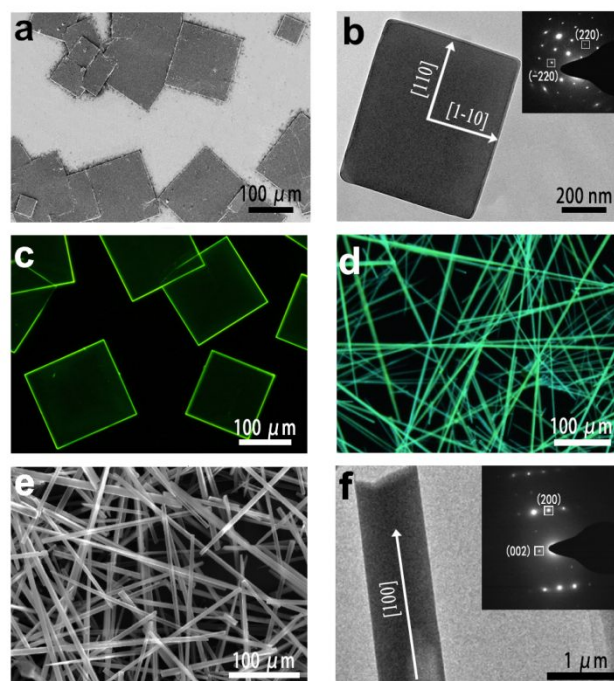

Figure 2. (a, e) SEM, (c, d) Fluorescence microscopy (FM), and (b, f) TEM images of (a, b, c) BP microsheets and (d, e, f) BP-1,3-DTFB microwires. Insets shown in b and f present the corresponding SAED patterns, respectively.

1
2
3
4
5
6
7
8
9
10
11
12
13
14
15
16
17
18
19
20
21
22
23
24
25
26
27
28
29
30
31
32
33
34
35
36
37
38
39
40
41
42
43
44
45
46
47
48
49
50
51
52
53
54
55
56
57
58
59
60

Unexpectedly, BP microsheets would transform into nanorod meshes upon immersing them into 1,3-DTFB solution in isopropyl alcohol (IPA, C_{DTFB} = 100 mM) and then slow evaporation of the suspension. Notably, two sets of vertically oriented nanorod arrays are connected together, giving 2D nanorod meshes with a width of around 150 μm and a diameter of a few hundred nanometers (Figure 3a, b). Moreover, small-sized BP sheets with a width of around 50 μm can also generate 2D nanorod meshes (Figure S6). Instead, partial transformation is achieved upon decreasing the concentration of 1,3-DTFB (C_{DTFB} = 50 mM) or increasing the evaporation rate of IPA (Figure S7). Under UV excitation, the nanorod arrays present cyan light (Figure 3a). We also collected the PL spectra of three BP-based assemblies to obtain detailed optical properties (Figure 3c). Specifically, BP microsheets show a main PL band at around 528 nm, which match well with green emission. Besides, BP-1,3-DTFB microwires present a PL band at 505 nm, which corresponds to cyan light. BP-1,3-DTFB wires displays a blue-shift PL band (23 nm) relative to that of BP sheets.
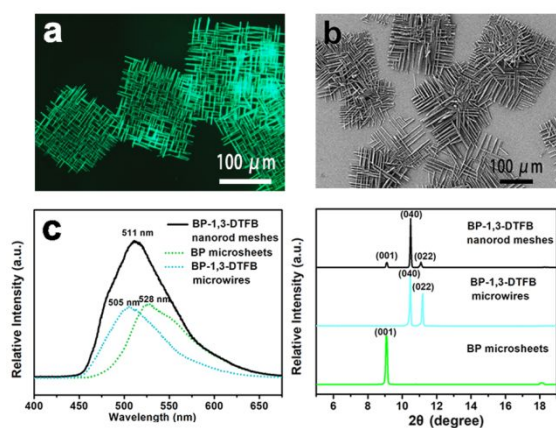

Figure 3. (a) FM and (b) SEM images of BP-1,3-DTFB nanorod meshes. (c) PL spectra and (d) PXRD patterns of three BP-based assemblies.

As described earlier, CT interaction in organic cocrystals commonly results in red-shifted PL, while AF interaction leads to blue-shifted PL.[8] Hence, cooperative CT and AF interactions should be responsible for blue-shifted PL of BP-1,3-DTFB wires. The BP-1,3-DTFB nanorod meshes exhibits a wide PL spectrum, which may be regarded as a sum of those of BP sheets and BP-1,3-DTFB wires. We hereby infer that a small amount of BP microsheets have not been completely transformed into nanorod arrays.

To further determine the composition of the nanorod meshes, we examined powder XRD patterns of the above three BP-based assemblies (Figure 3d). Typically, the characteristic peaks of BP microsheets and BP-1,3-DTFB microwires match well with their respective SCXRD patterns. The peaks of the nanorod meshes correspond to (040) and (022) planes of BP-1,3-DTFB as well as weak (001) plane of BP, further revealing the existence of a small portion of unconverted BP sheets. Compared to that of BP-1,3-DTFB wires, the peak intensity ratio of the nanorod meshes (I_{040}/I_{022}) increases dramatically, suggesting that the exposed (020) top/bottom facets of BP-1,3-DTFB nanorods.

Next, we aim to collect more structural information on crystal transformation by capturing the detailed evolution processes of 2D nanorod meshes at different growth stages. At t = 10 min, we can see that the BP microsheets with smooth appearance become rough, indicating the occurrence of etching (Figure 4a). At t = 60 min, partial regions of the BP sheets still keep intact and most of 1D nanorods are connected with each other to form discontinuous 2D nanorod meshes (Figure 4b). At t = 120 min, the BP microsheets were almost completely consumed and highly ordered nanorod meshes were clearly recognized (Figure 4c).

On the basis of the above results, two key issues may be proposed and clarified to reveal the formation mechanism of the nano-meshes: (i) What is the driving force for crystal transformation? (ii) How do 1D nanorods arrange themselves into ordered arrays? First, it seems reasonable to suppose that stronger CT and AF interactions between BP and 1,3-DTFB relative to π-π interaction between BP-BP drive crystal transformation. In particular, BP is nearly insoluble in IPA, while 1,3-DTFB dissolves well. Upon immersion of BP microsheets into 1,3-DTFB solution in IPA, BP molecules would gradually dissociate and diffuse into the solution due to the emerging intermolecular interactions for BP and 1,3-DTFB in high concentrations. As IPA evaporates, free BP molecules would undergo co-crystallization with the neighboring 1,3-DTFB molecules, forming BP-1,3-DTFB rods/wires. Under this process, partially consumed BP sheets still remain intact and act as a sacrificial template to afford ordered growth of BP-1,3-DTFB nanorods. Moreover, we infer that BP molecules follow short-distance diffusion due to the lower solubility and migration rate in IPA, thus giving horizontal nanorods rather than vertical nanorods. Besides a majority of single-layer nanorod meshes, a small amount of multilayer nanorod meshes were also obtained (Figure S8), possibly due to local excessive concentration of 1,3-DTFB solution.[4c]

Figure 5. (a, b) FM images of BP-1,4-DTFB nanorod meshes at (a) low and (b) high magnification.
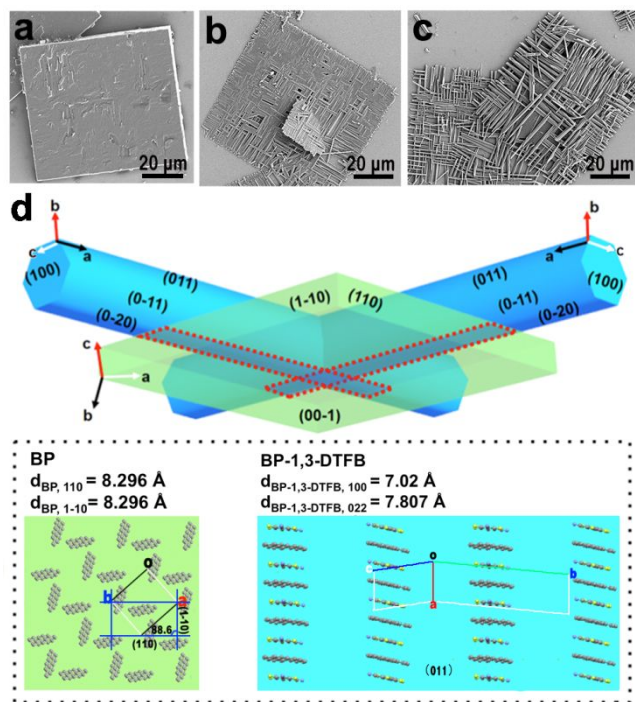

Figure 4. (a-c) The evolution processes of BP-1,3-DTFB nanorod meshes at different growth stages. (d) Top: schematic showing epitaxial growth of BP-1,3-DTFB nanorods on a BP microsheet at the junction region. Bottom: the molecular packing motifs of (left) BP and (right) BP-1,3-DTFB at this region.

Second, crystallographic epitaxial relationship between BP and BP-1,3-DTFB was evaluated to reveal the cause of oriented nanorod arrays. We construct a schematic diagram of nanorod meshes at the junction region (Figure 4d), where the *ab*-plane of BP and the *ac*-plane of BP-1,3-DTFB are joined together. At this region, the molecular arrangement of BP microsheet and BP-1,3-DTFB nanorod is revealed. In BP crystal, BP molecules are stacked along [110] and [1-10] directions with equivalent lattice distances ($d_{110} = d_{1-10} = 8.296$ Å). BP and 1,3-DTFB in BP-1,3-DTFB cocrystal are stacked alternately along CT direction with exposed (011) side facets ($d_{022} = 7.807$ Å). Notably, $d_{BP-1,3-DTFB, 011}$ is nearly twice as much as $d_{BP, 110}$ or $d_{BP, 1-10}$. Close lattice spacing between BP and BP-1,3-DTFB enables desired lattice matching ($f = 5.9\%$), thus leading to epitaxial growth of 100-oriented BP-1,3-DTFB nanorods on BP microsheet. Considering that the side facets of BP microsheet are enclosed by equivalent (110)/(1-10) planes, the emerging BP-1,3-DTFB nanorods would arrange themselves into orthogonal nanorod arrays with a horizontal orientation.
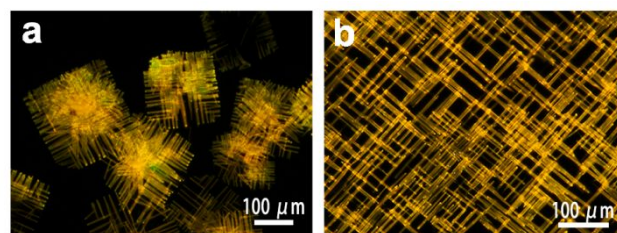
Such a crystal transformation strategy was also extended to the fabrication of nanorod meshes comprising BP-1,4-DTFB with 1:1 stoichiometry (Figure 5). Specifically, BP microsheets still act as a template and undergo crystal transformation to form BP-1,4-DTFB nanorod superstructures. In contrast to cyan-emitting BP-1,3-DTFB nano-meshes, BP-1,4-DTFB nano-meshes present yellow light under UV excitation. We infer that stronger CT and AF interactions between BP and 1,4-DTFB than those between BP and 1,3-DTFB lead to longer-wavelength emission of BP-1,4-DTFB, as verified by its PL spectrum (Figure S6a). Similarly, small lattice mismatch between BP and BP-1,4-DTFB ($f = 4.1\%$) enables epitaxial growth of BP-1,4-DTFB nanorods. Moreover, partially or fully converted 2D nanorod meshes comprising BP-octafluoronaphthalene (BP-OFN, Figure S10) or BP-1,2,4,5-tetracyanobenzene and (BP-TCNB, Figure S11) were also achieved by transformation of BP microsheets. Thus, crystal transformation has been demonstrated to be a general strategy to achieve aligned nanorod superstructures.

In summary, we develop a crystal transformation strategy for rational synthesis of organic nanorod meshes, where the pre-existing 2D microsheets serve as a sacrificial template to allow epitaxial growth of nanorods. The transformation was driven by cooperative intermolecular interactions between an electron D/A pair. Desired lattice matching between 2D microsheet and 1D cocrystal nanorod enables the formation of nanorod arrays. By elaborate selection of electron acceptors, 2D nanorod meshes with different luminescence were achieved readily. As exemplified in CsPbBr$_3$ nanowire networks, PL can propagate from one branch to another and a strong cavity coupling exists at the wire junctions.[9] Considering high structural similarity, such a phenomenon may also exist in luminescent BP-based nanorod meshes, what makes them promising candidates for optoelectronic devices such as optical waveguiding and photodetectors.

ASSOCIATED CONTENT

Supporting Information

Detailed experimental procedures and characterization. This material is available free of charge via the Internet at http://pubs.acs.org.

AUTHOR INFORMATION

Corresponding Author

wai-yeung.wong@polyu.edu.hk.
yilonglei@tju.edu.cn.

Notes
The authors declare no competing financial interests.

ACKNOWLEDGMENT

REFERENCES

(1) (a) Wang, Y.; Torres, J. A.; Stieg, A. Z.; Jiang, S.; Yeung, M. T.; Rubin, Y.; Chaudhuri, S.; Duan, X.; Kaner, R. B. Graphene-Assisted Solution Growth of Vertically Oriented Organic Semiconducting Single Crystals. *ACS Nano* **2015**, *9*, 9486–9496. (b) Zheng, J. Y.; Xu, H. J.; Wang, J. J.; Winters, S.; Motta, C.; Karademir, E.; Zhu, W. G.; Varrla, E.; Duesberg, G. S.; Sanvito, S.; Hu, W. P.; Donegan, J. F. Vertical Single-Crystalline Organic Nanowires on Graphene: Solution-Phase Epitaxy and Optical Microcavities. *Nano Lett.* **2016**, *16*, 4754–4762. (c) Zhao, Y. S.; Wu, J.; Huang, J. Vertical Organic Nanowire Arrays: Controlled Synthesis and Chemical Sensors. *J. Am. Chem. Soc.* **2009**, *131*, 3158–3159. (d) Zhao, Y. S.; Zhan, P.; Kim, J.; Sun, C.; Huang, J. X. Patterned Growth of Vertically Aligned Organic Nanowire Waveguide Arrays. *ACS Nano* **2010**, *4*, 1630–1636. (e) Tang, Q.; Li, H.; Song, Y.; Xu, W.; Hu, W.; Jiang, L.; Liu, Y.; Wang, X.; Zhu, D. In Situ Patterning of Organic Single-Crystalline Nanoribbons on a SiO$_2$ Surface for the Fabrication of Various Architectures and High-Quality Transistors. *Adv. Mater.* **2006**, *18*, 3010-3014. (f) Li, H.; Tee, B. C.-K.; Cha, J. J.; Cui, Y.; Chung, J. W.; Lee, S. Y.; Bao, Z. High-Mobility Field-Effect Transistors from Large-Area Solution-Grown Aligned C$_{60}$ Single Crystals. *J. Am. Chem. Soc.* **2012**, *134*, 2760–2765. (g) Zhang, C. Y.; Zhang, X. J.; Zhang, X. H.; Fan, X.; Jie, J. S.; Chang, J. C.; Lee, C-S.; Zhang, W. J.; Lee, S.-T. Facile One-Step Growth and Patterning of Aligned Squaraine Nanowires via Evaporation-Induced Self-Assembly. *Adv. Mater.* **2008**, *20*, 1716–1720. (h) Su, B.; Wang, S. T.; Ma, J.; Wu, Y. C.; Chen, X.; Song, Y. L.; Jiang, L. Elaborate Positioning of Nanowire Arrays Contributed by Highly Adhesive Superhydrophobic Pillar-Structured Substrates. *Adv. Mater.* **2012**, *24*, 559–564.

(2) Zhang, Y.; Diao, Y.; Lee, H.; Mirabito, T. J.; Johnson, R. W.; Puodziukynaite, E.; John, J.; Carter, K. R.; Emrick, T.; Mannsfeld, S. C. B.; Briseno, A. L. Intrinsic and Extrinsic Parameters for the Growth of Organic Single-Crystalline Nanopillars in Photovoltaics. *Nano Lett.* **2014**, *14*, 5547–5554.

(3) (a) Wu, Y. C.; Feng, J. G.; Jiang, X. Y.; Zhang, Z.; Wang, X. D.; Su, B.; Jiang, L. Positioning and Joining of Organic Single-Crystalline Wires. *Nat. Commun.* **2015**, *6*, 6737–6746. (b) Deng, W.; Zhang, X. J.; Wang, L.; Wang, J. C.; Shang, Q. X.; Zhang, X. H.; Huang, L. M.; Jie, J. S. Wafer-Scale Precise Patterning of Organic Single-Crystal Nanowire Arrays via A Photolithography-Assisted Spin-Coating Method. *Adv. Mater.* **2015**, *27*, 7305–7312.

(4) (a) Li, L. S.; Sun, N. J.; Huang, Y. Y.; Qin, Y.; Zhao, N. N.; Gao, J. N.; Li, M. X.; Zhou, H. H.; Qi, L. M. Topotactic Transformation of Single-Crystalline Precursor Discs into Disc-Like Bi$_2$S$_3$ Nanorod Networks. *Adv. Funct. Mater.* **2008**, *18*, 1194–1201. (b) Guo, C. F.; Cao, S. H.; Zhang, J. M.; Tang, H. Y.; Guo, S. M.; Tian, Y.; Liu, Q. Topotactic Transformations of Superstructures: From Thin Films to Two-Dimensional Networks to Nested Two-Dimensional Networks. *J. Am. Chem. Soc.* **2011**, *133*, 8211–8215. (c) Lei, Y. L.; Wang, S. Y.; Lai, Z. C.; Yao, X.; Zhao, Y. L.; Zhang, H.; Chen, H. Y. Two-Dimensional C$_{60}$ Nano-Meshes via Crystal Transformation. *Nanoscale* **2019**, *11*, 8692–8698.

(5) Lei, Y. L.; Sun, Y. Q.; Zhang, H. Y.; Liao, L. S.; Lee, S.-T.; Wong, W.-Y. Facet-Selective Growth of Organic Heterostructured Architectures via Sequential Crystallization of Structurally Complementary π-Conjugated Molecules. *Nano Lett.* **2017**, 17, 695–701.

(6) (a) Imoto, M.; Ikeda, H.; Fujii, T.; Taniguchi, H.; Tamaki, A.; Takeda, J.; Mizuno, K. Contrasting Intermolecular and Intramolecular Exciplex Formation of a 1,4-Dicyano-2-methylnaphthalene-*N,N*-Dimethyl-*p*-toluidine Dyad. *Org. Lett.* **2010**, *12*, 1940–1943. (b) Eisuke, O.; Hitoshi, K.; Atsushi, S.; Yasunori, M.; Hiroyasu, S.; Hiroshi, I. Fluorescence Behavior Associated with a Possible Intercolumnar Charge-Transfer Interaction in the Crystalline State of a Dyad Consisting of Mesitylene and 1,4-Dicyano-2-methylnaphthalene Subunits. *Rapid Commun. Photosci.* **2015**, *4*, 31–33. (c) Sarma, M.; Wong, K.-T. Exciplex: An Intermolecular Charge-Transfer Approach for TADF. *ACS Appl. Mater. Interfaces* **2018**, *23*, 19279–19304. (d) Imoto, M.; Ikeda, H.; Ohashi, M.; Takeda, M.; Tamaki, A.; Taniguchi, H.; Mizuno, K. Control of the CT Interaction between Electron-Donor and -Acceptor Moieties of a 1,4-Dicyanonaphthalene-arene Dyad for Intermolecular Exciplex or Excimer Formation in Crystals. *Tetrahedron Lett.* **2010**, *51*, 5877–5880. (e) Belova, V.; Beyer, P.; Meister, E.; Linderl, T.; Halbich, M.-U.; Gerhard, M.; Schmidt, S.; Zechel, T.; Meisel, T.; Generalov, A. V.; Anselmo, A. S.; Scholz, R.; Konovalov, O.; Gerlach, A. V.; Anselmo, A. S.; Scholz, R.; Konovalov, O.; Gerlach, A.; Koch, M.; Hinderhofer, A.; Opitz, A.; Brütting, W.; Schreiber, F. Evidence for Anisotropic Electronic Coupling of Charge Transfer States in Weakly Interacting Organic Semiconductor Mixtures. *J. Am. Chem. Soc.* **2017**, *139*, 8474–8486. (f) Jin, X.-H.; Chen, C.; Ren, C.-X.; Cai, L.-X.; Zhang, J. *Chem. Commun.* **2014**, *50*, 15878–15881.

(7) (a) Hori, A.; Shinohe, A.; Yamasaki, M.; Nishibori, E.; Aoyagi, S.; Sakata, M. 1:1 Cross-Assembly of Two β-Diketonate Complexes through Arene-Perfluoroarene Interactions. *Angew. Chem. Int. Ed.* **2007**, *46*, 7617–7620. (b) Sharber, S. A.; Baral, R. N.; Frausto, F.; Haas, T. E.; Müller, P.; Thomas III, S. W. Substituent Effects That Control Conjugated Oligomer Conformation through Non-covalent Interactions. *J. Am. Chem. Soc.* **2017**, *139*, 5164–5174.

(8) Sun, Y. Q.; Lei, Y. L.; Liao, L. S.; Hu, W. P. Competition between Arene-Perfluoroarene and Charge-Transfer Interactions in Organic Light-Harvesting Systems. *Angew. Chem. Int. Ed.* **2017**, *56*, 10352–10356.

(9) Chen, J.; Fu, Y. P.; Samad, L.; Dang, L.; Zhao, Y.; Shen, S.; Guo, L.; Jin, S. Vapor-Phase Epitaxial Growth of Aligned Nanowire Networks of Cesium Lead Halide Perovskites (CsPbX$_3$, X = Cl, Br, I). *Nano Lett.* **2017**, *17*, 460–466.

1
2
3
4
5
6
7
8
9
10
11
12
13
14
15
16
17
18
19
20
21
22
23
24
25
26
27
28
29
30
31
32
33
34
35
36
37
38
39
40
41
42
43
44
45
46
47
48
49
50
51
52
53
54
55
56
57
58
59
60

Epitaxial Growth of Nanorod Meshes from Luminescent Organic Cocrystals via Crystal Transformation